A β-Naphthaleneimide-Modified Terthiophene Exhibiting Charge Transfer and Polarization Through the Short Molecular Axis. Joint Spectroscopic and Theoretical Study

Sandra R. González, Juan Casado,* and Juan T. López Navarrete*

Department of Physical Chemistry, University of Málaga, Campus de Teatinos s/n, Málaga 29071, Spain

Raúl Blanco and José L. Segura*

Department of Organic Chemistry, Complutense University of Madrid, Faculty of Chemistry, Madrid 28040, Spain

Received: March 14, 2008; Revised Manuscript Received: April 17, 2008

We present a new terthiophene derivative substituted at the thienyl β positions with a naphthalenediimide functionalization. The UV−vis absorption and emission spectroscopic properties as well as the electrochemical properties have been discussed to describe its electronic structure. The vibrational Raman data are used to inspect the molecular architecture. All of the experimental data are supported by quantum chemical calculations with different approaches. A close comparison with other terthiophenes available in the literature is conducted, always stressing the effect of the relative orientation of the donor and acceptor groups either with long-axis or short-axis polarizations. The electronic structure of the molecule has been understood in terms of the HOMO−LUMO absolute energy values. A considerable reduction of the band gap from the constituting units to the studied molecule is detected, although electronic interaction is not optimal for this configuration. Fluorescence quenching is interpreted by the possibility of intersystem crossing and internal conversion. Finally, Raman spectroscopy gives additional information of the distribution of conjugation along the molecular domain, of subtle conformational effects, and of the intermolecular interaction by means of temperature-dependent Raman data. This study provides guidelines for controlling the electronic structure and for exploring new strategies pursuing improved dyes.

I. Introduction

Oligo- and polythiophenes are among the best investigated and most frequently used conjugated materials, in particular, as active components in organic electronic devices and molecular electronics.[1,2] For example, they are used as light-emitting diodes (OLEDs) or lasers,[3] field-effect transistors (OFETs),[4] integrated circuits, and solar cells (OSCs).[5] On the other hand, monodisperse oligomers have received a great deal of attention in recent years given that they are excellent model compounds for the corresponding polydisperse polymers which include chain length distributions, defects, and interruptions of the conjugated chains.[6] Valuable structure−property relationships and extrapolations to the polymer have been established by monitoring different properties that depend on the chain length, which is the so-called oligomeric approach.[7] With this aim, for almost all basic conjugated polymers, the corresponding oligomers have been produced.[2] In this way, the field of organic electronics and optoelectronics has developed into a double approach: (i) the attainment of conjugated polymers processed from solutions by monomer polymerization and (ii) the use of well-defined conjugated oligomers built up by step-by-step organic synthesis and typically processed by more costly evaporation techniques. Despite their easier processability and less demanding synthetic work, the use of polymers includes disadvantages (i.e., less-defined molecular structures and less defect-free thin films) leading to an uninterrupted growing and development of the parent monodisperse oligomeric materials. Thus, since the discovery of polythiophene in 1981 by Tourillon and Garnier,[8] many smaller oligothiophenes have been synthesized, such as those extensively reviewed by Roncali,[9–11] Zotti,[12] Pomerantz,[13] Bryce et al.,[14] and Swager et al.[15,16]

Among oligothiophenes, donor (D)−acceptor (A) derivatives receive a great deal of attention due to their ambipolar field-effect charge transport[17–19] and their use in organic photovoltaics. Thus, recently, D−A-based ter- and quaterthiophenes **1** (n = 1, 2) (Chart 1) endowed with *N*-ethylcarbazole and cyanoacrylic acid at each terminus were prepared for their utilization as active components in dye-sensitized solar cells (DSSCs) with an incident photon-to-current conversion efficiency (IPCE) of ∼70% in the range of 400−650 nm and good maximum power conversion efficiencies of 7.7 and 5.6% under AM 1.5 illumination.[20]

Oligothiophenes end-capped with cyano (**2**)[21–23] or cyano-containing groups, such as dicyanovinylene (**3**),[24] tricyanovinylene (TCV) (**4**, **5**)[25,26] and dicyanomethylene (**6**),[23,27–31] were prepared and investigated (Chart 1). The incorporation of these electron-withdrawing groups into oligothiophene backbones induced strong bathochromic shifts in their optical spectra and lowered the HOMO−LUMO gap (i.e., HOMO: highest occupied molecular orbital; LUMO: lowest unoccupied molecular orbital). Leo and Bäuerle et al. recently reported the synthesis of low-band-gap acceptor-capped oligothiophenes designed for the use in bilayer heterojunction solar cells (**7**, Chart 1), showing a maximum power conversion efficiency of 3.4% under illumination with simulated sunlight.[32,33] For these device applications, it is crucial to control the electronic structure of the material in order to achieve (a) a band gap of the desired magnitude and

* To whom correspondence should be addressed. E-mail: casado@uma.es.

10.1021/jp802228a CCC: $40.75
Published on Web 06/27/2008

CHART 1: Selected Donor−Acceptor Oligothiophenes

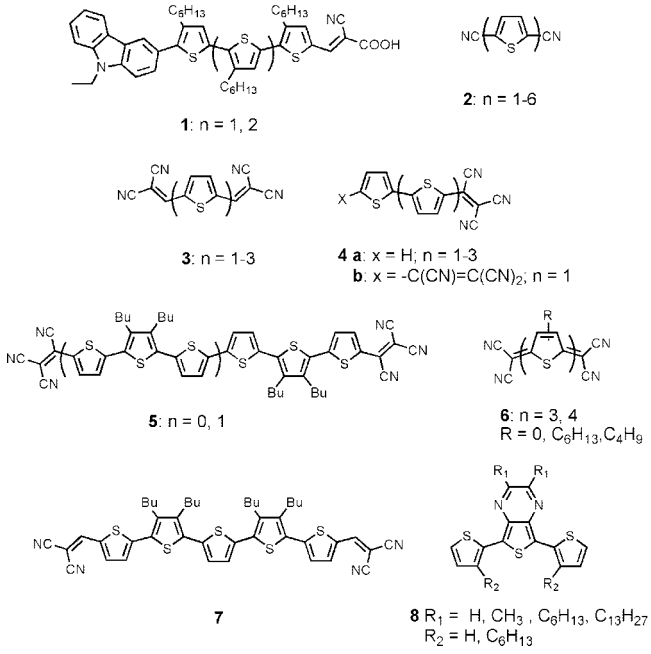

(b) a HOMO and LUMO with appropriate energies.[34] One different approach to obtain D−A oligothiophenes as low-band-gap materials involves the alternation of electron-donating and electron-accepting moieties in conjugated co-oligomers,[35] showing that the mixing of monomer segments with a higher HOMO and a lower LUMO is effective to reduce the band gap due to the intrachain charge transfer (i.e., ICT).[36,37] Thus, a number of trimeric thiophene derivatives **8** (Chart 1) have been synthesized with the middle thiophene unit fused with pyrazine moieties. Relatively high electron mobility and ambipolar field-effect charge transport have been recently observed in this kind of thiophene-based donor−acceptor oligomer.[38] However, the inclusion of strong electron-withdrawing groups, which favor extensive ICT, might be detrimental for charge transport since the undesired confinement or localization of the injected charge, hence less electron-withdrawing groups able to efficiently delocalized the extra charge, can provide an interesting strategy to optimize the final output as far as charge stabilization and transport are concerned. We will show here an example of such an alternative.

In an attempt to control the electronic properties (band gap and HOMO/LUMO energies) and to promote efficient ambipolar charge transport within the hypothesis of combining electron and hole extended conjugated (i.e., electron-delocalized) units, we propose the synthesis of a naphthaleneamidinemonoimide derivative fused with a terthiophene moiety through an imidazole unit (**NPTI-3T**, Figure 1). The 1,4,5,8-naphthalenetetracarboxylic acid diimides are important compounds for materials and supramolecular chemistry.[39] Since naphthalenediimides are easily reversibly reduced to form stable radical anions, they serve as electron-acceptor units in artificial photosynthetic systems for solar energy conversion.[40] In addition, the introduction of arylimidazole to extend the conjugation in rylene-type derivatives is an efficient strategy to red shift the absorption of these dyes.[41] Thus, the novel **NPTI-3T** is designed to absorb light in the whole UV−vis region.

In this paper, we will describe the synthesis of **NPTI-3T**, which is the starting point for a deep analysis of **NPTI-3T**, paying special attention to the features of its electronic and molecular structures in order to achieve a complete understanding of its spectral, photophysical, and electrochemical properties that, as already mentioned, definitively decide its suitable use in applications. The potential exploitation of **NPTI-3T** as a polymerizable monomer is not central now and will deserve careful study elsewhere. Our main goals can be summarized as (i) a comparative evaluation of the **NPTI-3T** properties relative to other donor−acceptor oligothiophenes, choosing those with well-differentiated electron-withdrawing strength (i.e., **TCV-3T** in Figure 1) and extended topology in the electronic interaction (i.e., **PRI-3T** in Figure 1), and (ii) of prime interest for us is also the property evolution as a function of the step-by-step addition of chemical building blocks (i.e., **3T**, **NPTI**, and **NPTI-1T** in Figure 1) and the inspection of spectroscopic−structure relationships. To this goal, a paralleled experimental and theoretical study is proposed for every property analyzed. Electronic absorption and emission spectroscopies together with electrochemistry are used for the electronic structure discussion (section III), and Raman spectroscopy gives us information about the molecular structure (section IV). DFT and time-dependent DFT theories are used for the simulation of the experimental data and to guide the interpretation. The excited states discussion will require the use of the RCIS-HF approach.

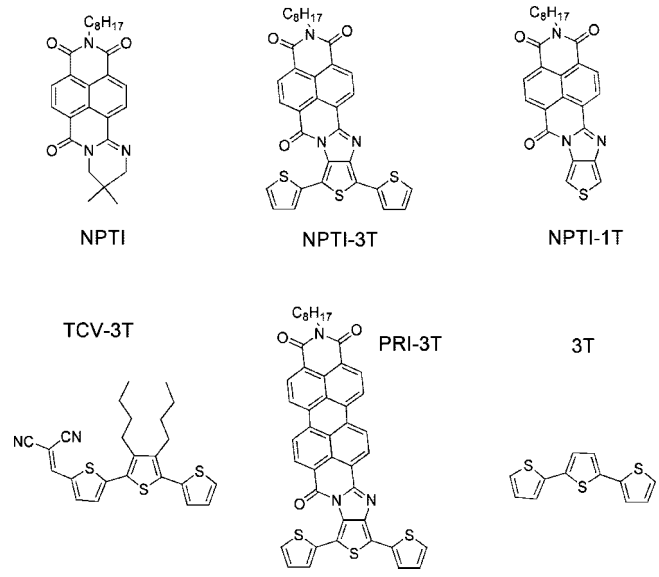

Figure 1. Chemical structures of the studied compounds, including intermediates and references.

II. Experimental and Theoretical Details

II. 1. Synthesis. The synthesis of this type of compound can be carried out by reaction of *o*-phenylenediamines with anhydrides derived from naphthalene- or perylenedicarboxylic acids.[42] By following this strategy (Scheme 1), we synthesized naphthaleneamidinemonoimideterthiophene (**NPTI-3T**), the parent naphthaleneamidinemonoimidethiophene (**NPTI-1T**), as well as the reference **NPTI** prepared for comparison purposes. See Supporting Information for additional synthetic details and characterization data (NMR, mass spectra, etc.) of the new products.

II. 2. Electrochemistry. Cyclic voltammetry experiments were performed with a computer-controlled EG & G PAR 273 potentiostat in a three electrode single-compartment cell (5 ml). The platinum working electrode consisted of a platinum wire sealed in a soft glass tube with a surface of $A = 0.785$ mm^2, which was polished down to 0.5 μm with Buehler polishing paste prior to use in order to obtain reproducible surfaces. The

SCHEME 1: Synthesis of the Compounds

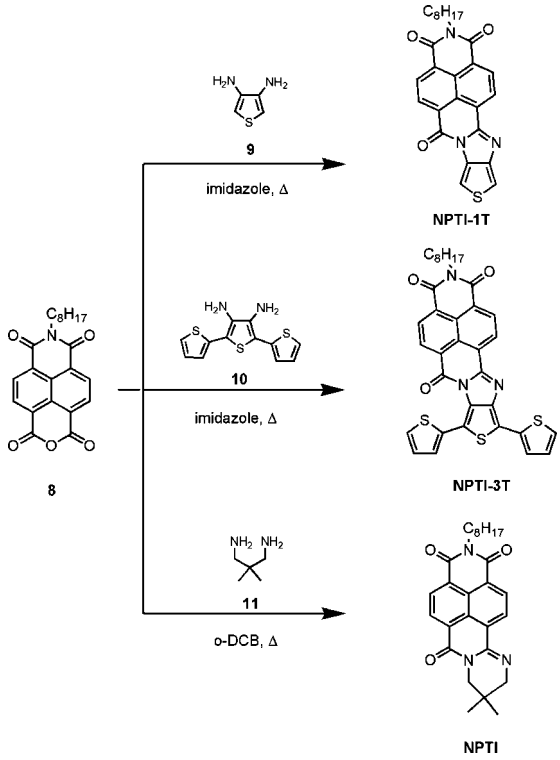

counter electrode consisted of a platinum wire, and the reference electrode was a Ag/AgCl secondary electrode. All potentials were internally referenced to the ferrocene−ferricenium couple. For the measurements, concentrations of 5×10^{-3} mol L^{-1} of the electroactive species were used in freshly distilled and deaerated dichloromethane (Lichrosolv, Merck) and 0.1 M tetrabutylammonium hexafluorophosphate (TBAHFP, Fluka), which was twice recrystallized from ethanol and dried under vacuum prior to use.

II. 3. Spectroscopic Details. UV−vis absorption spectra were recorded on an Agilent 8453 instrument equipped with a diode array detection system. Emission spectra were measured using a JASCO FP-750 spectrofluorometer. No fluorescent contaminants were detected upon excitation in the wavelength region of experimental interest. FT-Raman scattering spectra were collected on a Bruker FRA106/S apparatus and a Nd:YAG laser source ($\lambda_{exc} = 1064$ nm) in a back-scattering configuration. The operating power for the exciting laser radiation was kept to 100 mW in all of the experiments. Samples were analyzed as pure solids averaging 1000 scans with 2 cm^{-1} of spectral resolution. Resonance Raman spectra ($\lambda_{exc} = 532$ nm) were recorded by using a Senterra dispersive Raman microscope from Bruker.

II. 4. Calculations. Ground-state total energies, equilibrium geometries, eigenfrequencies, and normal coordinates were calculated using Density Functional Theory by means of the Gaussian-03 package of programs.[43] The Becke's three parameter (B3) gradient-corrected exchange functional combined with the correlation Lee−Yang−Parr (LYP) functional was utilized.[44] The 6-31G** basis set was used.[45] Theoretical Raman spectra were obtained for the resulting ground-state optimized geometries; harmonic vibrational frequencies and Raman intensities were calculated analytically and numerically, respectively.[46] The time-dependent DFT (TD-DFT) approach has been used for the evaluation of at least the 10 lowest-energy vertical electronic excited states including both singlet and triplet states.[47] TD-DFT calculations were performed using the same functional (B3LYP) and basis set (6-31G**). The geometry optimization of the first excited S_1 state was carried out using the ab initio method restricted configuration interaction singles (RCIS)[48] incorporated in the Gaussian 03W software and using the 6-31G* basis. TD-DFT/B3LYP/6-31G** calculations were used to calculate the $S_1 \rightarrow S_0$ electronic excitations from the RCIS-optimized (relaxed) S_1 state.

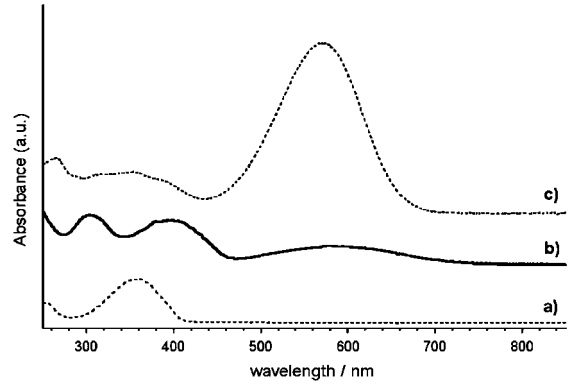

Figure 2. UV−vis spectra of a) **3T**, b) **NPTI-3T**, and c) **TCV-3T** in CH_2Cl_2.

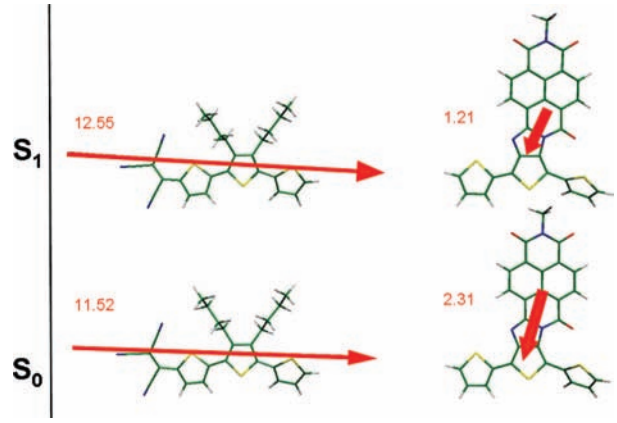

Figure 3. DFT//B3LYP/6-31G** dipolar momentum vectors (in red, the modulus in Debye) for the S_0 ground and S_1 excited states of **NPTI-3T** and **TCV-3T**.

III. Electronic Spectra and Electronic Structure

III. 1. Absorption Spectra. Figure 2 displays the electronic absorption spectrum of **NPTI-3T** in CH_2Cl_2. TD-DFT/B3LYP/6-31G** calculations have been carried out for the S_0 ground electronic state and vertical electronic excitations obtained in order to compare with the UV−vis experimental data.

Three important bands are recorded for **NPTI-3T** in CH_2Cl_2 at 583, 397, and 302 nm that might be related to the theoretical excitations at 738, 468−419, and 359−340 nm, respectively. Calculated oscillator strengths for the three features are 0.21 (738 nm), 0.34 (468−419 nm), and 0.40 (359−340 nm), which qualitatively agree with the tendency of the molar extinction coefficients of the experimental bands, or 6.04×10^3 (583 nm), 1.51×10^4 (397 nm), and 1.78×10^4 (302 nm), respectively. The broad absorption at 583 nm is typically of an intramolecular charge-transfer band (i.e., ICT). This is theoretically confirmed since it can be described as a HOMO → LUMO one-electron excitation that consists of the displacement of the electron density from the HOMO mostly located at the terthiophene unit to the LUMO mainly described by the naphthalene unit. There

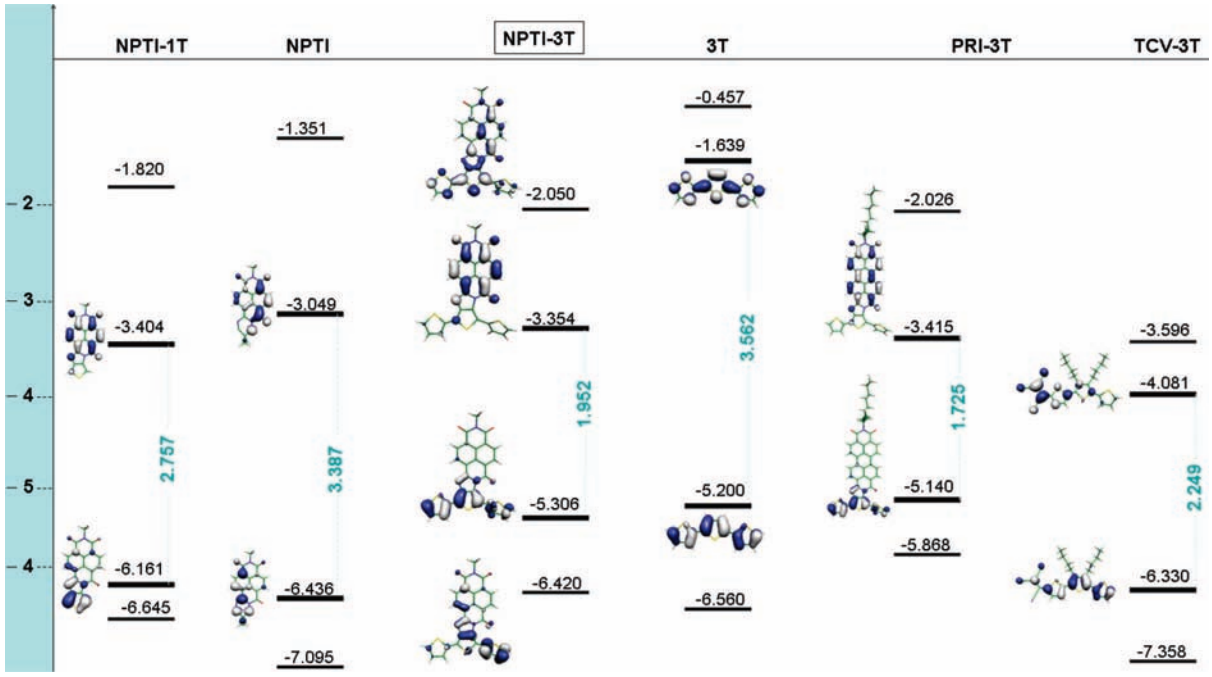

Figure 4. DFT/B3LYP/6-31G** frontier orbitals and absolute energies (in eV) for the compounds under study.

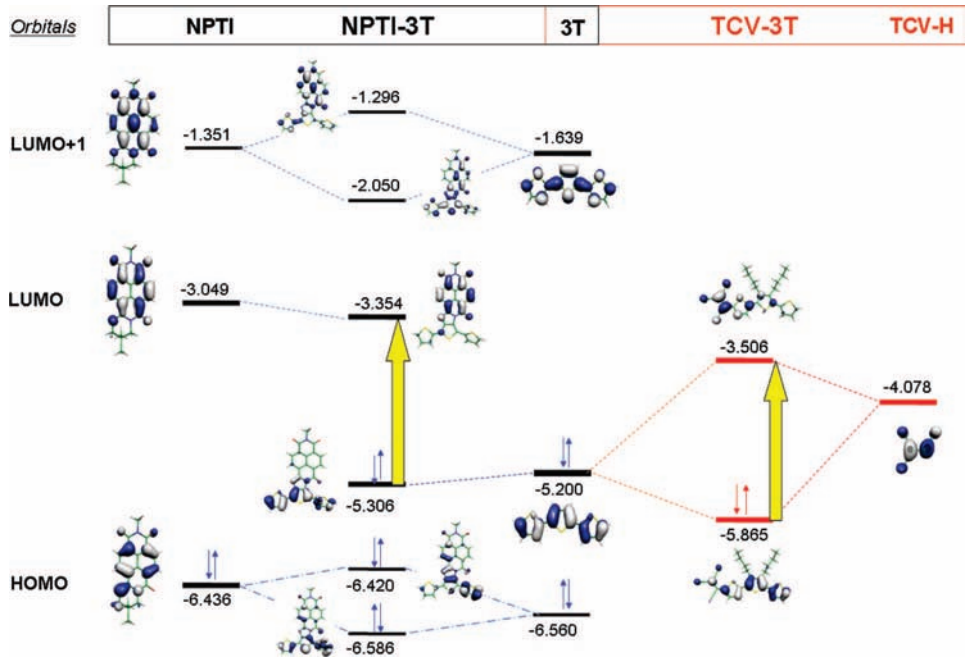

Figure 5. B3LYP/6-31G** molecular orbital diagram (energies in eV) of the coupling between the **NPTI**, **3T**, and **TCV-H** fragments giving rise to **NPTI-3T** and **TCV-3T**. Arrows in yellow indicate the HOMO−LUMO gaps.

is a very moderate overlapping of the two wavefunctions (central thiophene and imidazol) along the excitation which explains the lowest predicted oscillator strength and intensity of this ICT band among the absorptions.

Also in Figure 2, the UV−vis absorption spectra of **NPTI-3T** and that of **TCV-3T** (i.e., α-tricyanovinylterthiophene as an example of a push−pull terthiophene having substitution with an electron acceptor at one terminal α position of the thienyl chain) are compared. In **TCV-3T**, donor-to-acceptor ICT nominally occurs along the long molecular axis from the α point to the **3T**, in contrast with the path through the β connections in **NPTI-3T**.[49] In **TCV-3T**, the lowest-energy ICT band, also due to a HOMO → LUMO excitation, is the strongest of the spectrum due to the maximal overlapping of the heteroaromatic HOMO and heteroquinoid LUMO along the oligothiophene moiety, which also contrasts with the rather small HOMO−LUMO wavefunction superposition in **NPTI-3T**.

The directions of the dipolar momentum vectors in Figure 3 nicely show the different topology of the ICT in the two molecules: along the long terthiophene molecular axis for **TCV-3T** and over the short molecular axis for **NPTI-3T**. It is deduced that the small atomic coefficients at the β positions in these orbitals limit electronic communication or conjugation between the two moieties in **NPTI-3T**, while the large atomic coefficients at α favor electron delocalization.

Figure 4 depicts the electronic levels and correlation for the orbitals around the gap, stressing their evolution with chemical substitution. Comparing the orbital topologies of **3T** and **NPTI-**

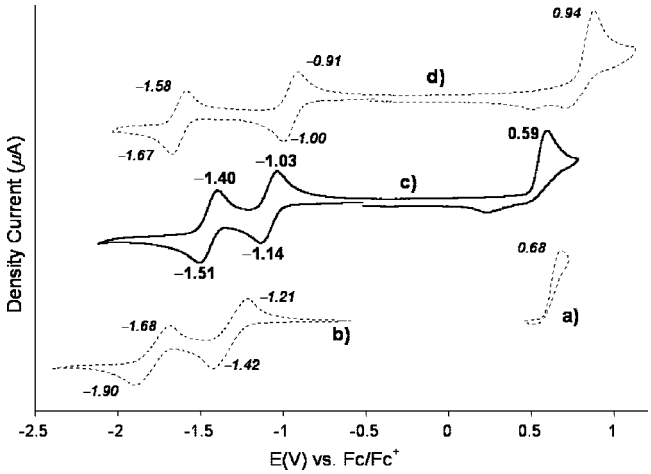

Figure 6. Cyclic voltammetries of a) **3T**, b) **NPTI**, c) **NPTI-3T**, and d) **TCV-3T**.

3T, it is deduced that both HOMOs correlate; however, the LUMO of **3T** is similar to the LUMO+1 of **NPTI-3T**, meaning that the LUMO of the latter seems to be a energy level inserted in the prohibited gap of the neutral **3T**. Thus, the LUMO of the **NPTI** unit mainly becomes the LUMO of **NPTI-3T**. This invokes the situation after doping of conducting polymers wherein accessible electronic states in the gap are responsible for the properties of doped polymers.

Relative to **NPTI-3T**, the reduction/enlargement of the HOMO−LUMO gap in **NPTI-1T/PRI-3T** is a consequence of the HOMO/LUMO destabilization/stabilization on **1T** → **3T**/**NPTI** → **PRI** due to better conjugation in the larger molecular systems. These simple arguments are valid because of the small electronic delocalization between both benzene- and thiophene-based units, which permits treatment of the frontier orbitals almost separately. This is nicely visualized in Figure 5, where a possible combination of the frontier orbitals of the building blocks is proposed to account for the energies and topologies of the frontier orbitals of **NPTI-3T**. While the HOMO and LUMO of **NPTI-3T** come from the isolated HOMO and LUMO of **3T** and **NPTI**, respectively, the lower and higher terms can be expressed by combinations of the corresponding orbitals. This description differs from that of **TCV-3T**, where its HOMO and LUMO are combinations of the HOMO and LUMO of **3T** and **TCV**, reflecting a great orbital mixing.[49] However, their similar HOMO → LUMO excitation energies (571 nm in **TCV-3T** and 583 nm in **NPTI-3T**) do not reflect the different interaction through α and β positions. It seems that the greater delocalization ability in **NPTI** balances the stronger mesomeric effect (i.e., electron-withdrawing) of **TCV**, which indeed offers, in relative terms, a restricted electron delocalization path given its small size.

The situation described in the above section can be explained by arguing the limited communication through the β positions of the thiophene. However, the optimized geometry of S_0 displays a considerable distortion of the external thiophene which is close to the carbonyl group; this ring greatly rotates, likely to mitigate steric crowding (this effect will be more carefully analyzed in section IV). The combination of these two effects might be the origin of the appearance of the "isolated" HOMO and LUMO of **NPTI-3T**, in contrast with the extensive orbital mixing in **TCV-3T**. On the other hand, the HOMO of **3T** and the LUMO of **TCV** combine, giving rise to the HOMO of **TCV-3T** that provokes an electron occupation of the former LUMO of **TCV** at the expense of the electron density of the former HOMO of **3T**, which results in a strong charge polarization of the ground electronic state (see the dipolar momentum vector). In **NPTI-3T**, however, its HOMO is almost the HOMO of **3T**, and the phenomenon of charge redistribution is absent, and its dipolar momentum vector is thus small.

III. 2. Electrochemical Properties. Figure 6 shows the cyclic voltammetries of the studied compounds. **NPTI-3T** displays both cathodic and anodic processes that can be interpreted in the framework of the Koopmann's approach since reduction and oxidation occur on the LUMO and HOMO orbitals, respectively. According to the above electronic structure description, electron extraction happens on the **3T** unit, which, due to high activity (great HOMO orbital and spin atomic coefficients) of its free α-terminal positions, leads to polymerization provoking the irreversibility of the wave. Reduction instead involves the naphthalene unit and is stabilized in **NPTI-3T** relative to **NPTI**, in accordance with the more stable LUMO orbital in the former (see Figure 5). The very strong electron-withdrawing tricyanovinyl group displaces the oxidation of **TCV-3T** by 0.34 V at higher potentials. The first reduction process in **TCV-3T** is stabilized by 0.10 V, while the second one is destabilized by 0.18 V compared to **NPTI-3T**. Moreover, the redox windows (i.e., electrochemical gap) also differ in both samples, 1.85 and 1.62 V in **TCV-3T** and **NPTI-3T**, respectively. These electrochemical properties indicate that, depending on the topology and nature of the substitutions with acceptors, significant differences in the absolute energy position of the HOMO and LUMO are attained. This energy modulation is very important in the energetics of the coupling of the molecule with the metallic electrodes (i.e., work functions) of the device.

III. 3. Photophysical Properties. No emission spectra were obtained for **NPTI-3T** upon excitation on its absorption bands. Upon light absorption, and assuming that the Kasha rule applies, it is the structure of the S_1 emitting state which determines the subsequent relaxation steps, which involve either photon emission to the S_0 (i.e., fluorescence), intersystem crossing to the triplet manifold, internal conversion, or exciton rupture and formation of charge separate states (i.e., electrons and holes), potentially leading by migration to photovoltaic action. According to the complete fluorescence quenching detected experimentally, the analysis of the S_1 state and exploration of its electronic properties toward the understanding of the favored de-excitation routes become relevant.

RCIS/HF/6-31G*-optimized geometries of the S_1 state have been obtained for the compounds under analysis. On the S_1-optimized structures, new TD-DFT//B3LYP/6-31G** calculations have been carried out, and the HOMO → LUMO excitation has been taken as the representative transition associated with the fluorescence or radiative properties (see Figure 7). In this approach, we take the DFT-optimized geometry for the S_0 and the RCIS for the S_1; thus, in Figure S1, we provide a photophysical theoretical scheme, similar to that of Figure 7, in which TD-DFT excitation energy calculations were done over the HF S_0- and RCIS-HF S_1-optimized geometries. In Figures S2 and S3, the HF(S_0)/RCIS-HF(S_1) and DFT(S_0)/RCIS-HF(S_1) theoretical data are compared with the absorption and emission properties for **3T** and **NPTI-3T**. For **3T**, excitation to S_1 provokes two main structural changes: (i) quinoidization of the conjugated C=C/C−C path and (ii) planarization of the inter-ring structure. In **NPTI-3T**, the most noticeable changes are concerned with the quinoidization of the bithiophene segment already planarized in the ground electronic state (see section IV), while the distorted thiophene significantly modifies neither its CC bonds nor its dihedral angle with the central ring. These

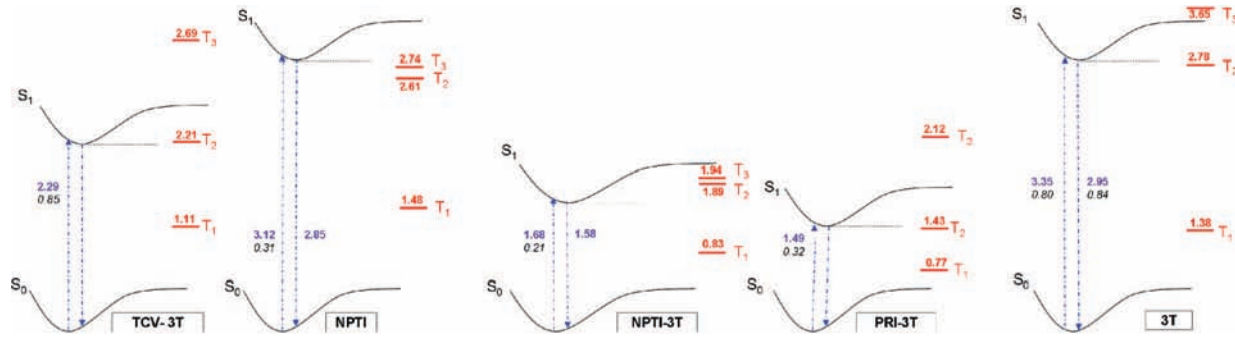

Figure 7. Theoretical photophysical properties of the studied molecules. TD-DFT/B3LYP/6-31G** singlet and triplet energies are shown in eV.

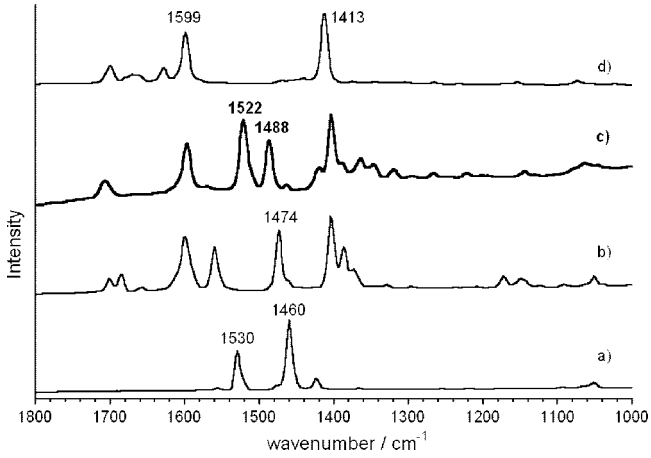

Figure 8. FT-Raman spectra of a) **3T**, b) **NPTI-1T**, c) **NPTI-3T**, and d) **NPTI**.

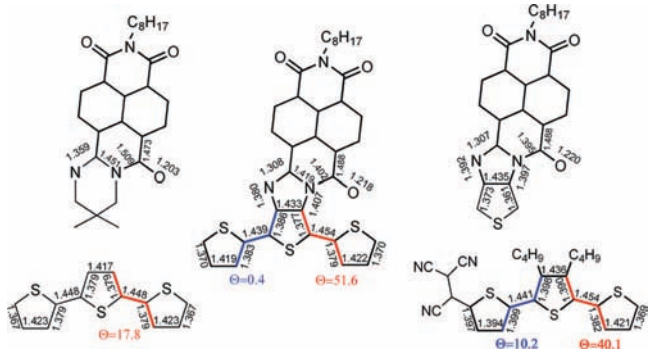

Figure 9. More relevant DFT//B3LYP/6-31G** geometrical parameters (lengths in Å) on the optimized geometries of the studied compounds.

geometrical data are in line with the smaller theoretical Stokes shift predicted theoretically for **NPTI-3T** (0.10 eV) compared with that for **3T** (0.40 eV). However, similar Stokes shifts of 0.35−0.40 eV are calculated for the constituting units **NPTI** and **3T**. From an energetic point of view, this small reorganization energy in **NPTI-3T** upon photoexcitation makes the exciton binding energy in the diabatic S_1 state more favorable for charge separation and photovoltaic action. In the α-to-α′ push−pull **TCV-3T**, structural reorganization in S_1 is also small compared to that in S_0, and the most significant change is concerned with the dihedral angle between the central and the non-TCV-connected thiophene, 35.5° for S_0 and 22.4° in S_1. This description regarding the small reorganization energies (i.e., theoretical Stokes shifts) in the two charge-transfer molecules (i.e., **TCV-3T** and **NPTI-3T**) is in agreement with the absence of vibronic structure in the so-termed absorption bands at the lowest energies. Indeed, **NPTI** and **3T** show distinctive vibronic activity.

Regarding the fluorescence properties, **3T** displays reasonably high quantum yields; however, full fluorescence quenching is observed in **NPTI-3T**. It is known that one of the main mechanisms of fluorescence quenching in oligothiophenes is intersystem crossing to the triplet manifold; hence, the presence of accessible triplet excited states can open the way for $S_1 \rightarrow T_n$ energy transfer in our molecules. This process is controlled by two main parameters: (i) spin-orbit coupling and (ii) the energy difference between the closest triplet state to S_1, $\Delta E(S_1-T_n)$ or exchange energy. At the optimized geometry of this S_1 state, vertical triplet excited states have been calculated and included in Figure 7. The largest $\Delta E(S_1-T_n) = 0.75$ eV in the series corresponds to **NPTI-3T**, and one would anticipate that intersystem crossing is limited in this case under exclusive consideration of the adiabatic energy. Consequently, and aside from intermolecular phenomena, the more feasible mechanism for the observed quenching would be the nonradiative $S_1 \rightarrow S_0$ internal conversion, especially effective in low-band-gap molecules; of the studied molecules, full quenching of the photoluminescence is observed in the systems with the lowest S_1-S_0 gap, or **NPTI-3T**, **TCV-3T**, and **PRI-3T**.

IV. Vibrational Raman Spectra and Molecular Structure

IV. 1. FT-1064-Raman Spectra. Figure 8 shows the Raman spectra of **NPTI-3T** together with those of their constituent building blocks. The Raman spectrum of **3T** is characterized by two important bands at 1530 and 1460 cm^{-1} that correspond to thiophene ν(C=C) vibration modes of the terminal and innermost rings, respectively.[50] On the other hand, the Raman spectrum of the naphthalenimide moiety has two strong features at 1599 and 1413 cm^{-1}. Upon connection of both groups in **NPTI-3T**, the lines mainly affected are those assigned to the terthiophene moiety that now appear at 1522 (1530 cm^{-1} in **3T**) and 1488 cm^{-1} (1460 cm^{-1} in **3T**), whereas the most noticeable change on the **NPTI** moiety is the 1413 → 1404 cm^{-1} on **NPTI** → **NPTI-3T**.

These vibrational changes can be interpreted as a function of the geometrical modifications so that Figure 9 compares the DFT/B3LYP/6-31G**-optimized geometries of **NPTI**, **3T**, and **NPTI-3T**. As for the terthiophene moiety, a strong distortion of the dihedral angle between one of the two outermost thiophenes (i.e., that close to the carbonyl group) and the central ring is noticed, with a value of 51.6 versus 17.8° in **3T**. However, the homologue angle on the other side of the molecule is strongly planarized (0.7°) in **NPTI-3T** compared to that in **3T** (17.8°). This asymmetric distortion arises from a steric and/

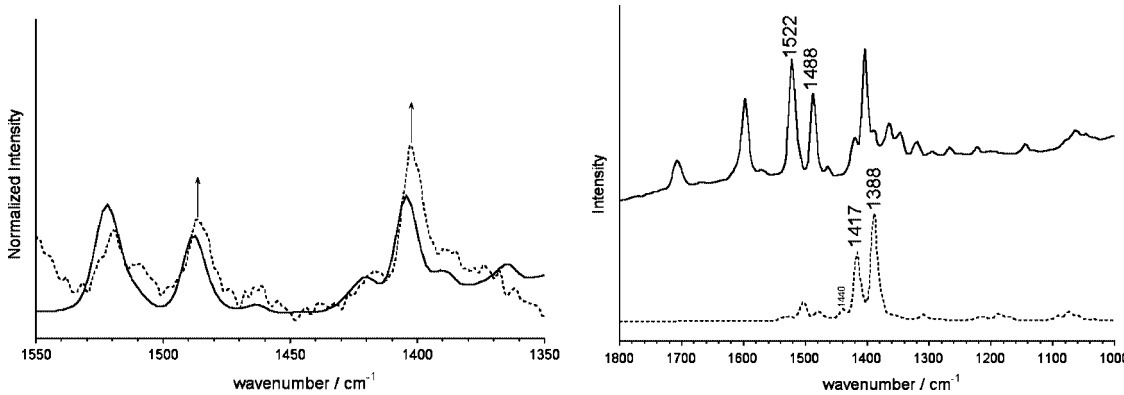

Figure 10. Left: 1064 nm (bold line) and resonance 532 nm (dotted line) Raman spectra of **NPTI-3T**. Right: FT-Raman spectra of **NPTI-3T** (top) and **TCV-3T** (bottom).

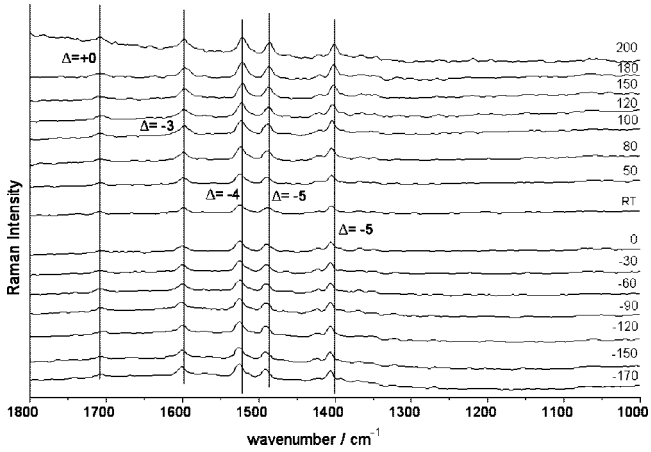

Figure 11. The 1064 nm FT-Raman spectra of **NPTI-3T** as a function of the temperature (°C, RT: room temperature). Wavenumber increments (Δ), calculated as the highest minus lowest temperature wavenumbers, are given in cm^{-1}.

TABLE 1: Frequencies and Wavenumber Variation Δ (Highest Minus Lowest Temperature Wavenumbers) in cm^{-1} of the Most Important Raman Bands of the 1064 nm FT-Raman Spectrum of Some of the Studied Molecules

	NPTI-3T	TCV-3T	3T
wavenumber-1/δ	1708/+0		
wavenumber-2/δ	1598/−3		
wavenumber-3/δ	1522/−4	1440/−5	1530/−2
wavenumber-4/δ	1488/−5	1417/−3	1460/−1
wavenumber-5/δ	1404/−5	1388/−7	

or electronic repulsion between the electronic clouds of oxygen (i.e., carbonyl group) and sulfur (i.e., thiophene).

It is generally established that the strongest Raman lines in oligothiophenes downshift or upshift their frequencies when more efficient or interfered conjugation occurs. Taking this structural information into account, the 1530(**3T**) → 1522(**NPTI-3T**) frequency downshift might result from the increase/decrease of the C═C/C−C bond lengths in the terminal ring, which is almost planarized with the central one. A possible explanation for the behavior of the bands at 1460 cm^{-1} in **3T** and 1488 cm^{-1} in **NPTI-3T**, or the frequency upshift upon substitution, is concerned with the topology of the blockade of the two central β positions of terthiophene. If conjugation in **3T** is exclusively linear, or one sequence of conjugating C═C/C−C bonds from the α position to the other α′ position, the inclusion of **NPTI** adds a new path for electronic delocalization which is cross conjugated with the linear one. The interference of both paths, together with the conformational distortion already described, makes the overall electronic communication less efficient in **NPTI-3T** than that in **3T**, and as a result, the strong terthiophene Raman line upshifts its frequency by 18 cm^{-1}. However, paying attention to the particular CC bond lengths, some discrepancies are apparent. Despite the electronic isolation by rotation of the terminal distorted thiophene, its CC bond distances are similar to those of the other terminal thienyl ring (i.e., one would anticipate that better conjugation with the central ring would soften its skeletal structure, as occurs with the dihedral angle). This structural resemblance arises from two opposite effects, on one hand, the effectiveness of conjugation in the case of the planar outer thiophene and, on the other, the antibonding character on the HOMO wavefunction for the C═C double bonds of this distorted ring which weaken and consequently lengthen.

IV. 2. Resonance Raman Spectra and Linear versus Cross Conjugation. A more detailed analysis of the effect of cross conjugation can be made by considering the Raman signal associated with the electronic HOMO → LUMO transition which describes the β coupling giving rise to the cross-conjugated path. In order to get this information, the Raman spectrum with a laser excitation of 532 nm was taken, which coincides with the electronic absorption associated with the HOMO → LUMO promotion measured at 583 nm.

This resonance Raman spectrum is shown in Figure 10. Since the HOMO is centered at the terthiophene and the LUMO is at the naphthalene moiety, the resonance Raman signal relatively enhances the **3T** and **NPTI** conjugating vibrational modes (i.e., CC stretching modes) which mimic the evolution dictated by the corresponding HOMO/LUMO wavefunctions; the 1488 and 1404 cm^{-1} bands are enhanced.

Figure 10 also compares the FT-Raman spectra of **NPTI-3T** and **TCV-3T**, showing an important displacement at lower frequencies for the relevant terthiophene bands of **TCV-3T**.[49] A strong quinoidization of the terthiophene molecular structure occurs in **TCV-3T**, which is responsible for the ∼100 cm^{-1} frequency downshift relative to **NPTI-3T**. For example, the thiophene ring connected to the **TCV** group has its three CC bond distances almost equal. This spectroscopic data, well supported by theoretical geometries, indicates that the strong electron-withdrawing **TCV** group removes part of the charge density in the terthiophene (i.e., less significant for further rings), leading to its quinoidization. However, given the nature of the "isolated" frontier orbitals in **NPTI-3T**, such donor → acceptor charge drain is absent, and quinoidization is much less noticeable.

IV. 3. Thermospectroscopic Study. Figure 11 displays the FT-Raman spectra of **NPTI-3T** as a function of temperature in

the solid state, whereas Table 1 summarizes the temperature variation of the strongest lines of **NPTI-3T**, **TCV-3T**, and **3T**. The samples show a good thermal stability; no drastic changes are detected in the range of temperatures analyzed, and the spectra reversibly recover at any temperature. The most noticeable finding is the frequency upshift of the thiophene and naphthalene lines by 5 cm^{-1} upon cooling, while the carbonyl band remains unaltered. Similar upshifts have been reported for oligothiophenes with the lowering of the temperature, which have been related to the compression of the crystallographic unit cell at low temperatures by strengthening of the intermolecular forces.[51] This effect leads to an alteration of the intermolecular potential and therefore of the vibrational frequencies. The largest frequency changes are detected for the π-conjugating Raman lines indicating cofacial $\pi-\pi$ intermolecular contacts and that this coupling undergoes a slight modification with temperature. Largest changes are observed for **TCV-3T**, indicating that (i) $\pi-\pi$ intermolecular overlap by π stacking is more extensive in more quinoidal molecules (i.e., **TCV-3T**) wherein intermolecular spacing is lower; this is clearly exemplified in the case of a completely quinoid tertiophene (Chart 1, $n = 3$) with an upshift up to 10 cm^{-1} upon going from +200 to −170 °C,[51] and (ii) for heteroaromatic systems such as **3T**, on one hand, the molecule is already planar and the $\pi-\pi$ intermolecular distances in the unit cell are rather large such that small compression (i.e., by cooling and intermolecular force strengthening) scarcely affects the intermolecular potential.[52]

V. Conclusions

We have conceived and synthesized a new terthiophene derivative substituted at β positions with a naphthalenemonoimide functionalization, pursuing the attainment of new physical properties. The UV−vis spectroscopic and electrochemical properties are discussed in connection with its electronic structure, while the vibrational Raman data outline the molecular structure of the sample. Quantum chemical calculations are carried out with several methodologies to support and discuss the experimental data. A close comparison with other terthiophenes available in the literature is done, and the effect of the relative orientation of the donor and acceptor groups, or topology, is inspected.

The weak intramolecular donor-to-acceptor charge transfer is a consequence of minimal electronic interaction of the frontier orbitals of the building units upon connection in **NPTI-3T**, which leads to a minimal energy change in its HOMO and LUMO that can thus be viewed as "isolated" orbitals or practically not altered regarding its starting subunits. Hence, the HOMO−LUMO excitation results in intramolecular charge-transfer character and weak intensity. This situation is opposite to the pattern of orbital combination in **TCV-3T**. In this sense, the electrochemical properties reflect this situation since **NPTI-3T** keeps the ability of reduction of its **NPTI** homologues while oxidations are slightly destabilized; amphoteric redox behavior is retained for the sample. The photophysical properties are characterized by a red-shifted absorption band which is still weak in intensity in comparison to **TCV-3T** and that must be intensified for more optimal solar-to-current energy conversion. Fluorescence is quenched for **NPTI-3T**, and a possible explanation conceiving the activity of the nearest triplet excited states and the S_1-S_0 low band gap is presented. Raman spectroscopy is instrumental for the analysis of the molecular properties, in particular, gives experimental support to the distortion of the lateral thiophene ring relative to the remaining bithiophene fragment. This molecular feature must be modified in further terthiophenes because of its impact in the HOMO/LUMO energy distribution and related effects. Interunit conjugation or electron delocalization has been examined by the vibrational Raman properties.

Summarizing, a dual perspective of substitution of oligothiophenes with electron-withdrawing groups either with long-axis or short-axis polarization has been studied, and the implication in the electronic and molecular properties was analyzed in detail. These studies reveal the subtle interplay between the subunits according to the topology of the interaction and might provide guidelines for the optimization of key features in organic optoelectronic devices.

Acknowledgment. The present work was supported in part by the Dirección General de Enseñanza Superior (DGES, MEC, Spain) through research projects CTQ2006-14987-C02-01 and CTQ2007-604459. The authors are also indebted to Junta de Andalucía for the project FQM1678/2006 and to the Comunidad de Madrid/Complutense joint project CCG07-UCM/PPQ-2126 (Group Nr. 910759). J.C. is grateful to the MEC of Spain for an I3 professorship position of Chemistry at the University of Málaga. S.R.G. acknowledges the Junta de Andalucía for a FPI grant, and R.B. is indebted to the Comunidad de Madrid for a predoctoral fellowship.

Supporting Information Available: Details of the synthesis and characterization of the new products is provided. This material is available free of charge via the Internet at http://pubs.acs.org.

References and Notes

(1) Fichou, D. Ed. *Handbook of Oligo- and Polythiophenes*; Wiley-VCH: Weinheim, Germany, 1999.
(2) Müllen, K., Wegner, G. Eds. *Electronic Materials: The Oligomer Approach*; Wiley-VCH: Weinheim, Germany, 1998.
(3) Ackelrud, L. *Prog. Polym. Sci* **2003**, *28*, 875.
(4) Sirringhaus, H. *Adv. Mater.* **2005**, *17*, 2411.
(5) Gómez, R.; Segura, J. L. In *Handbook of Organic Electronics and Photonics*; Nalwa, H. S. Ed. American Scientific Publishers: Valencia, CA, 2007; Vol. 3.
(6) Garnier, F.; Horowitz, G.; Fichou, D. *Synth. Met.* **1989**, *28*, 705.
(7) Bäuerle, P. *Adv. Mater.* **1992**, *4*, 102.
(8) Tourillon, G.; Garnier, F. *J. Electroanal. Chem.* **1982**, *135*, 173.
(9) Roncali, J. *Chem. Rev.* **1997**, *97*, 173.
(10) Roncali, J. In *Handbook of Conducting Polymers*; Skotheim, T. A., Elsenbaumer, R. L., Reynolds, J. R. Eds.; Marcel Dekker: New York, 1998; p 311.
(11) Roncali, J. *J. Mater. Chem.* **1999**, *9*, 1875.
(12) Zotti, G. In *Handbook of Conductive Molecules and Polymers*; Nalwa, H. S., Ed. Wiley: New York, 1997; Vol. 2, p 137.
(13) Pomerantz, M. In *Handbook of Conducting Polymers*; Skotheim, T. A., Elsenbaumer, R. L., Reynolds, J. R. Eds.; Marcel Dekker: New York, 1998; p 277.
(14) Goldenberg, L. M.; Bryce, M. R.; Petty, M. C. *J. Mater. Chem.* **1999**, *9*, 1957.
(15) McQuade, D. T.; Pullen, A. E.; Swager, T. M. *Chem. Rev.* **2000**, *100*, 2537.
(16) Holliday, B. J.; Swager, T. M. *Chem. Commun.* **2005**, 23.
(17) Yoon, M.-H.; DiBenedetto, S. A.; Facchetti, A.; Marks, T. J. *J. Am. Chem. Soc.* **2005**, *127*, 1348.
(18) Ando, S.; Nishida, J.-I.; Tada, H.; Inoue, Y.; Tokito, S.; Yamashita, Y. *J. Am. Chem. Soc.* **2005**, *127*, 5336.
(19) Zaumseil, J.; Sirringhaus, H. *Chem. Rev* **2007**, *107*, 1296.
(20) Koumura, N.; Wang, Z. S.; Mori, S.; Miyashita, M.; Suzuki, E.; Hara, K. *J. Am. Chem. Soc.* **2006**, *128*, 14256.
(21) Barclay, T. M.; Cordes, A. W.; MacKinnon, C. D.; Oakley, R. T.; Reed, R. W. *Chem. Mater.* **1997**, *9*, 981.
(22) Melucci, M.; Barbarella, G.; Zambianchi, M.; DiPietro, P.; Bongini, A. *J. Org. Chem.* **2004**, *69*, 4821.
(23) Zotti, G.; Zecchin, S.; Vercelli, B.; Berlin, A.; Casado, J.; Hernandez, V.; Ortiz, R. P.; López Navarrete, J. T.; Orti, E.; Viruela, P. M.; Milian, B. *Chem. Mater* **2006**, *18*, 1539.

(24) Joshi, M. V.; Cava, M. P.; Lakshmikantham, M. V.; Metzger, R. M.; Abdeldayem, H.; Henry, M.; Venkateswarlu, P. *Synth. Met.* **1993**, *57*, 3974.

(25) Pappenfus, T. M.; Burand, M. W.; Janzen, D. E.; Mann, K. R. *Org. Lett.* **2003**, *5*, 1535.

(26) Bader, M. M.; Custelcean, R.; Ward, M. D. *Chem. Mater.* **2003**, *15*, 616.

(27) Higuchi, H.; Nakayama, T.; Koyama, H.; Ojima, J.; Wada, T.; Sasabe, H. *Bull. Chem. Soc. Jpn.* **1995**, *68*, 2363.

(28) (a) Pappenfus, T. M.; Chesterfield, R. J.; Frisbie, C. D.; Mann, K. R.; Casado, J.; Raff, J. D.; Miller, L. L. *J. Am. Chem. Soc* **2002**, *124*, 4184. (b) Janzen, D. E.; Burand, M. W.; Ewbank, P. C.; Pappenfus, T. M.; Higuchi, H.; Da Silva Filho, D. A.; Young, V. G.; Brédas, J.-L.; Mann, K. R. *J. Am. Chem. Soc.* **2004**, *126*, 15295.

(29) Janzen, D. E.; Burand, M. W.; Ewbank, P. C.; Pappenfus, T. M.; Higuchi, H.; Da Silva Filho, D. A.; Young, V. G.; Brédas, J.-L.; Mann, K. R. *J. Am. Chem. Soc.* **2004**, *126*, 15295.

(30) Takahashi, T.; Matsuoka, K.; Takimiya, K.; Otsubo, T.; Aso, Y. *J. Am. Chem. Soc.* **2005**, *127*, 8928.

(31) Ortiz, R. P.; Casado, J.; Hernández, V.; López Navarrete, J. T.; Ortí, E.; Viruela, P. M.; Milián, B.; Hotta, S.; Zotti, G.; Zecchin, S.; Vercelli, B. *Adv. Funct. Mater.* **2006**, *16*, 531.

(32) Schulze, K.; Uhrich, C.; Schüppel, R.; Leo, K.; M.; Pfeiffer, E.; Brier, E.; Reinold, P.; Bäuerle, *Proc. SPIE-Int. Soc. Opt. Eng.* **2006**, *6192*, 61920C-6.

(33) Schulze, K.; Uhrich, C.; Schüppel, R.; Leo, K.; Pfeiffer, M.; Brier, E.; Reinold, E.; Bäuerle, P. *Adv. Mater.* **2006**, *18*, 2872.

(34) (a) Thompson, B. C.; Kim, Y.-G.; McCarley, T. D.; Reynolds, J. R. *J. Am. Chem. Soc.* **2006**, *128*, 12714. (b) Galand, E. M.; Kim, Y.-G.; Mwaura, J. K.; Jones, A. G.; McCarley, T. D.; Shrotiya, V.; Yang, Y.; Reynolds, J. R. *Macromolecules* **2006**, *39*, 9132.

(35) Rasmussen, S. C.; Pomerantz, M. In *Handbook of Conducting Polymers*; Skotheim, T. A., Reynolds, J. R. Eds.; CRC Press: Boca Raton, FL, 2007; Chapter 12.

(36) (a) Kitamura, C.; Tanaka, S.; Yamashita, Y. *Chem. Mater.* **1996**, *8*, 570. (b) Casado, J.; Ponce-Ortiz, R.; Ruiz-Delgado, M. C.; Hernández, V.; López Navarrete, J. T.; Raimundo, J.-M.; Blanchard, P.; Allain, M.; Roncali, J. *J. Phys. Chem. B.* **2005**, *109*, 16616.

(37) Blanco, R.; Gómez, R.; Seoane, C.; Segura, J. L.; Mena-Osteritz, E.; Bäuerle, P. *Org. Lett.* **2007**, *9*, 2171.

(38) Nishida, J.-I.; Murakami, S.; Tada, H.; Yamashita, Y. *Chem. Lett.* **2006**, *35*, 1236.

(39) Röger, C.; Würthner, F. *J. Org. Chem.* **2007**, *72*, 8070.

(40) (a) Hasharoni, K.; Levanon, H.; Greenfield, S. R.; Gosztola, D. J.; Svec, W. A.; Wasielewski, M. R. *J. Am. Chem. Soc.* **1995**, *117*, 8055. (b) Greenfield, S. R.; Svec, W. A.; Gosztola, D.; Wasielewski, M. R. *J. Am. Chem. Soc.* **1996**, *118*, 6767. (c) Levanon, H.; Galili, T.; Regev, A.; Wiederrecht, G. P.; Svec, W. A.; Wasielewski, M. R. *J. Am. Chem. Soc.* **1998**, *120*, 6366. (d) Lukas, A. S.; Bushard, P.; Wasielewski, M. R. *J. Phys. Chem. A* **2002**, *106*, 2074. (e) Kelley, R. F.; Tauber, M. J.; Wasielewski, M. R. *J. Am. Chem. Soc.* **2006**, *128*, 4779. (f) Wasielewski, M. R. *J. Org. Chem.* **2006**, *71*, 5051. (g) Flamingi, L.; Baranoff, E.; Collin, J.-P.; Sauvage, J.-P. *Chem.—Eur. J.* **2006**, *12*, 6592.

(41) Adachi, M.; Nagao, Y. *Chem. Mater.* **1999**, *11*, 2107.

(42) Langhals, H.; Sprenger, S.; Brandherm, M.-T. *Liebigs Ann.* **1995**, 481.

(43) Frisch, M. J. Trucks, G. W.; Schlegel, H. B.; Scuseria, G. E.; Robb, M. A.; Cheeseman, J. R.; Montgomery, J. A., Jr.; Vreven, T.; Kudin, K. N.; Burant, J. C.; Millam, J. M.; Iyengar, S. S.; Tomasi, J.; Barone, V.; Mennucci, B.; Cossi, M.; Scalmani, G.; Rega, N.; Petersson, G. A.; Nakatsuji, H.; Hada, M.; Ehara, M.; Toyota, K.; Fukuda, R.; Hasegawa, J.; Ishida, M.; Nakajima, T.; Honda, Y.; Kitao, O.; Nakai, H.; Klene, M.; Li, X.; Knox, J. E.; Hratchian, H. P.; Cross, J. B.; Bakken, V.; Adamo, C.; Jaramillo, J.; Gomperts, R.; Stratmann, R. E.; Yazyev, O.; Austin, A. J.; Cammi, R.; Pomelli, C.; Ochterski, J. W.; Ayala, P. Y.; Morokuma, K.; Voth, G. A.; Salvador, P.; Dannenberg, J. J.; Zakrzewski, V. G.; Dapprich, S.; Daniels, A. D.; Strain, M. C.; Farkas, O.; Malick, D. K.; Rabuck, A. D.; Raghavachari, K.; Foresman, J. B.; Ortiz, J. V.; Cui, Q.; Baboul, A. G.; Clifford, S.; Cioslowski, J.; Stefanov, B. B.; Liu, G.; Liashenko, A.; Piskorz, P.; Komaromi, I.; Martin, R. L.; Fox, D. J.; Keith, T.; Al-Laham, M. A.; Peng, C. Y.; Nanayakkara, A.; Challacombe, M.; Gill, P. M. W.; Johnson, B.; Chen, W.; Wong, M. W.; Gonzalez, C.; Pople, J. A. *Gaussian 03*, revision B.05; Gaussian, Inc.: Pittsburgh, PA, 2003.

(44) Becke, A. D. *J. Chem. Phys.* **1993**, *98*, 1372.

(45) Francl, M. M.; Pietro, W. J.; Hehre, W. J.; Binkley, J. S.; Gordon, M. S.; Defrees, D. J.; Pople, J. A. *J. Chem. Phys.* **1982**, *77*, 3654.

(46) Scott, A. P.; Radom, L. *J. Phys. Chem.* **1996**, *100*, 16502.

(47) (a) Runge, E.; Gross, E. K. U. *Phys. Rev. Lett.* **1984**, *52*, 997. (b) Gross, E. K. U.; Kohn, W. *Adv. Quantum Chem.* **1990**, *21*, 255. (c) Gross, E. K. U.; Driezler, R. M. Plenum Press: New York, 1995.

(48) Foresman, J. B.; Head-Gordon, M.; Pople, J. A.; Frish, M. J. *J. Phys. Chem.* **1992**, *96*, 135.

(49) Casado, J.; Ruiz Delgado, M. C.; Rey Merchán, M. C.; Hernández, V.; López Navarrete, J. T.; Pappenfus, T. M.; Williams, N.; Stegner, W. J.; Johnson, J. C.; Edlund, B. A.; Janzen, D. E.; Mann, K. R.; Orduna, J.; Villacampa, B. *Chem.— Eur. J.* **2006**, *12*, 5458.

(50) Hernández, V.; Casado, J.; Ramírez, F. J.; Zotti, G.; Hotta, S.; López Navarrete, J. T. *J. Chem. Phys* **1996**, *104*, 9271.

(51) Casado, J.; Pappenfus, T. M.; Mann, K. R.; Ortí, E.; Viruela, P.M.; Milián, B.; Hernández, V.; López Navarrete, J. T. *ChemPhysChem.* **2004**, *5*, 529.

(52) (a) Fichou, D. *J. Mater. Chem.* **2000**, *10*, 571. (b) Hotta, S.; Waragai, K. J. *Mater. Chem.* **1991**, *1*, 835. (c) Graff, D. D.; Campbell, J. P.; Mann, K. R.; Miller, L. L. *J. Am. Chem. Soc.* **1996**, *118*, 5480. (d) Ramírez, F. J.; Aranda, M. A. G.; Hernández, V.; Casado, J.; Hotta, S.; López Navarrete, J. T. *J. Chem. Phys.* **1998**, *109*, 1920.

JP802228A